

# THE 4TH INTERNATIONAL CONFERENCE ON ALUMINUM ALLOYS

## THE EFFECT OF SILICON ON THE MICROSTRUCTURE AND PROPERTIES OF AA5182 ALLOY SHEET.

GJ Marshall, AJE Flemming & RA Ricks  
Alcan International Ltd, Banbury Laboratory, Southam Road,  
Banbury, Oxon OX16 7SP, UK.

### Abstract

The alloy AA5182 is extensively used for the manufacture of easy open beverage can ends from coil after cold rolling, lacquering and stoving. The ease of end making is related to many parameters; including end design, tooling condition and the surface and bulk material properties. Over the years, composition and sheet processing conditions have been determined to control mechanical properties and thus end formability.

Commercially, AA5182 is usually produced from high purity base metal to limit the levels of Fe and Si which historically have been linked to poor formability. Both elements lead to the formation of coarse constituent particles during ingot casting which persist during sheet production to final gauge and, it has been assumed, subsequently influence endstock formability.

The objective of the present study was to assess the effect of Si content, 0.08 to 0.33 wt%, on the evolution of microstructure during casting and sheet processing, and its influence on a wide range of mechanical properties. Detailed phase identification and quantitative metallography has been performed to correlate microstructure with endstock properties.

### Introduction

The ends for most of the world's beverage cans are made from the aluminium alloy AA5182 which nominally contains 4.5wt% Mg and 0.3wt% Mn. In considering a world market size of 150 billion cans every year, both aluminium and steel bodies, the vast majority have aluminium ends which indicates the importance of this product to the aluminium industry. The largest proportion of can ends, made from pre-lacquered coil, are manufactured through modern presses with production rates of ~600/min on each line. The choice of AA5182 is a compromise between strength, formability, sheet gauge and cost. Lacquered AA5182 is an expensive alloy but its inherent high strength after strain hardening allows thin gauges to be used. Contrary to can body manufacture, the precoating of endstock, which utilises a thermal curing operation, results in sheet

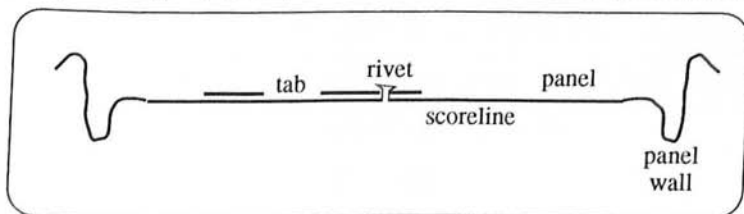


Figure 1: Schematic cross-section of a can end.

with the higher degree of formability needed to manufacture can ends. Figure 1 illustrates the key areas of the ends which require enhanced formability. The sheet encounters a range of strain paths to attain the correct end geometry; biaxial stretching for the rivet, plane strain compression of the scoreline and plane strain tension within the panel wall. High strength is also required to withstand the internal can pressures after filling and prevent end buckling. Typical minimum buckle pressure requirements are 85-90psi for soft drinks and 90-100psi for beers.

The combination of strength and formability has been achieved by selection of high Mg AA5182 which is formed in the bake softened condition but strain hardens during end making. The evolution of AA5182 can endstock (1) has meant a restriction in the levels of Fe and Si for reasons of formability. These elements lead to the formation of coarse constituent particles during solidification which survive ingot homogenisation to remain in the final product after break up during rolling. The general influence of coarse particles on tensile ductilities is well known (see reference 2 for Al-Mg alloys) and is often extrapolated to the formability of can ends. Little literature evidence exists to indicate what the tolerance of Fe and Si in AA5182 could be for this product.

The high level of Mg in AA5182 reduces the solubility of Si in aluminium to a negligible level (3) thus encouraging the formation of coarse Mg<sub>2</sub>Si particles. The purpose of the current work was to evaluate the effect of Si in can endstock over a large range designed to significantly change the sheet formability. It was felt that such a study could lead to a realistic tolerance level being set for Si and a better fundamental understanding of the influence of microstructure on performance.

### Materials

The compositions of the 3 alloys and the Aluminium Association (AA) specification, for comparison, are given in Table I. It should be noted, for the purpose of this investigation, that the high Si version, 0.33wt%, does not conform to the AA specification for AA5182. All other elements are typical of commercial AA5182 endstock and are within the AA specification.

Table I: Chemical Composition (wt%) of Trial Ingots. (\*maximum)

Version	Si	Fe	Cu	Mn	Mg	Zn	Ti
0.1%Si	0.08	0.22	-	0.32	4.67	-	0.003
0.2%Si	0.20	0.21	-	0.31	4.54	-	0.006
0.3%Si	0.33	0.21	-	0.32	4.67	-	0.002
AA spec.	0.20*	0.35*	0.15*	0.2-0.5	4.0-5.0	0.25*	0.10*

The alloys were commercially d.c. cast in Canada to produce 600mm thick x 4.2m long rolling ingots for rolling at an Alcan production facility in Germany. A typical hot rolling route through a reversing mill and a tandem mill produced a re-roll coil at ~2.5mm gauge. Cold rolling was performed

without an interanneal to the final gauge of 0.245mm prior to coil lacquering by Alcan Deutschland. Samples were obtained at ingot, hot rolled slab and re-roll coil and after cold rolling, before and after lacquering. These samples were used for detailed microstructural investigation to follow the evolution and break up of coarse particles and for laboratory formability evaluation.

Standard metallographic and property measurement techniques were employed during the investigation. However, phase identification was performed by x-ray diffraction on solvent extracted particles and quantitative metallography by Kontron image analysis on polished sections.

## Results and Discussion

### Microstructural Evolution.

Figure 2 shows optically the change in appearance of the coarse particles with increasing Si content. It should be apparent that the morphology of the Fe bearing phase (light grey) appears relatively unchanged whilst the  $Mg_2Si$  particles (black) have taken on a coarser, script morphology in the high Si variant. This change in morphology can be accounted for by the increased proportion of  $Mg_2Si$  and its solidification behaviour as a eutectic infilling at cell or grain boundary triple points. After extraction of the particles, SEM examination confirmed the morphology of the  $Mg_2Si$  but highlighted that the Fe phase exhibited 2 morphologies. Firstly, a similar shape to the  $Mg_2Si$  was seen but more prevalent at lower Si contents were feathery or acicular shaped clusters,

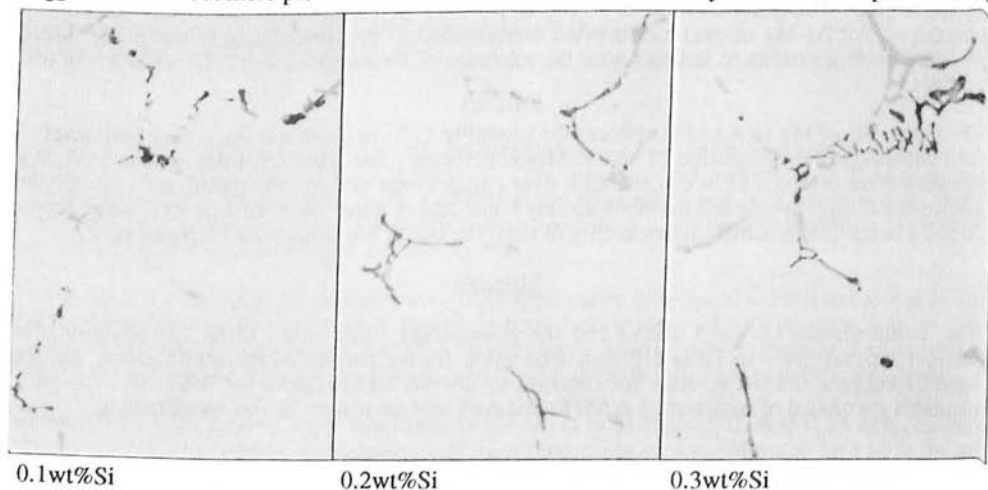


Figure 2: Effect of Si on the As Cast Microstructure of AA5182.

20µm

Phase identification was achieved using x-ray diffraction of the extracted particles and the results are summarised in Table II. In conjunction with the  $Mg_2Si$  phase, readily distinguished in optical metallography (figure 2), two Fe bearing phases were detected in the as cast microstructures and a third was formed during homogenisation. At low and medium Si contents the main intermetallic was  $(FeMn)_4Al_{13}$  with trace amounts of cubic  $Al_{15}(FeMn)_3Si_2$ . This trend switched in the high Si variant with only the cubic, Si containing phase detected, see Table II. During ingot homogenisation both as cast Fe phases partially transform to  $(FeMn)Al_6$  which appears to be the

Table II: Phase Identification from Extracted Coarse Intermetallic Particles.

Phase type	Low Si variant			Medium Si variant			High Si variant		
	Ingot	Homogn.	Final	Ingot	Homogn.	Final	Ingot	Homogn.	Final
$Mg_2Si$	√	√	√	√	√	√	√	√	√
$(FeMn)Al_6$	×	√	√	×	(√)	(√)	×	(√)	(√)
$(FeMn)_4Al_{13}$	√	√	√	√	×	×	×	×	×
$Al_{15}(FeMn)_3Si_2$	√	×	×	√	√	√	√	√	√

equilibrium phase at the homogenisation temperature, presumably stabilised by Mn. An additional assessment of the coarse particles at final, endstock gauge showed that no further significant change in phase type occurred during hot rolling. In addition to the coarse intermetallics, dispersoids form as part of the homogenisation treatment of the ingot, with both  $MnAl_6$  and  $Al_{15}Mn_3Si_2$  precipitating in the matrix. [The selection of filter size during extraction prevents the majority of the fine dispersoids from being collected].

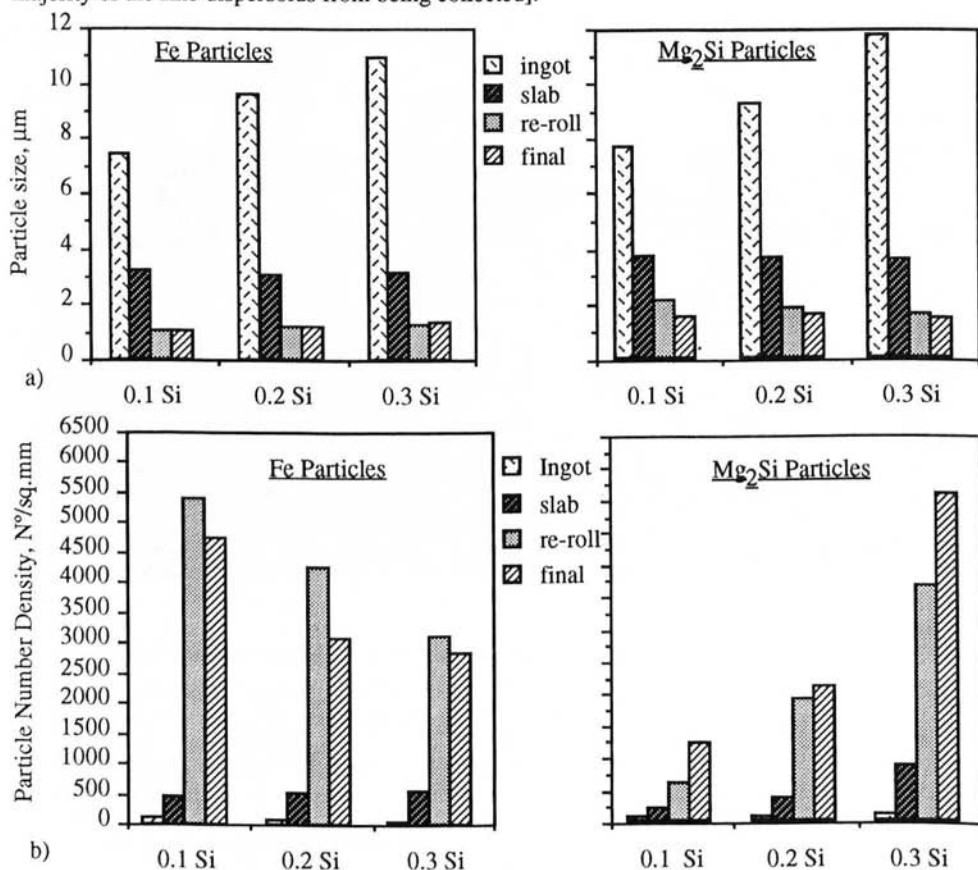


Figure 3: Effect of Si Content on (a) Coarse Particle Size and (b)  $N^\circ$  Density during Processing.

Quantitative metallography was performed on suitable samples at a variety of process stages to enable a study of the evolution of the coarse particle morphology and distribution. The area fraction of Fe phases was found to be 0.5-0.6%, independent of Si content, whilst the  $Mg_2Si$  area fraction was 0.2%, 0.5% and 1.0% with increasing Si content. Figure 3 shows that the Si level also alters the particle size of  $Mg_2Si$  in the as cast microstructure which again increases with Si. Somewhat more surprisingly, the increasing Si content also affects the size and  $N^\circ$  density of the Fe phases. The high Si variant, and to some extent the medium Si alloy, contains considerably fewer but substantially coarser Fe particles which x-ray diffraction indicated to be predominantly the cubic Si containing  $\alpha$ -phase. The break up of coarse particles during hot and cold rolling is only to be expected and in this manner the  $N^\circ$  density of particles will also dramatically increase.

In this respect, the  $Mg_2Si$  particles behave predictably with no discernible difference between variants in terms of particle size, although the  $N^\circ$  density at endstock gauge, figure 3, changed by a factor of 5 from the low to high Si variant. The results for the Fe phases were again not as expected, the difference seen in the as cast microstructures were reproduced at final gauge. At endstock gauge the average particle size increased from  $1.0\mu m$  to  $1.3\mu m$  with a concomitant reduction in the  $N^\circ$  density of particles. This only tells part of the story because the IBAS analysis uses a particle size cut-off of  $0.7\mu m$  (equivalent diameter) and hence smaller particle sizes are lost from the count. Figure 4 shows two scanning electron micrographs of particles extracted from final gauge variants containing 0.08wt% and 0.33wt% Si. These typical areas demonstrate quite clearly the significant difference in particle sizes that are not readily observed in the data from the image analyses.

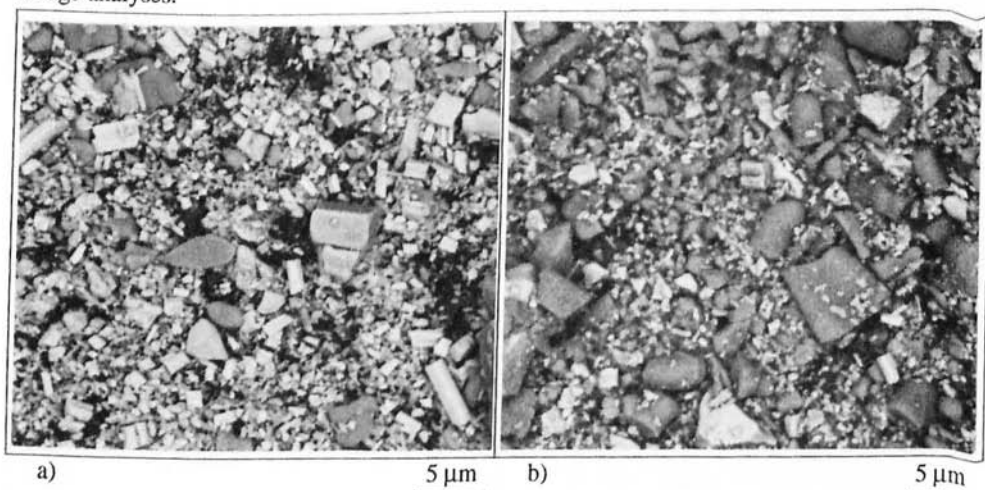


Figure 4: AA5182 endstock showing coarse particle size with a) 0.08wt% Si and b) 0.33wt% Si.

The conclusion can be reached that the variety of Fe phases present behave somewhat differently on two accounts. Firstly, during solidification the two major phases detected were  $(FeMn)_4Al_{13}$  and  $Al_{15}(FeMn)_3Si_2$ , depending upon Si content in the alloy, and their typical morphologies appear to be acicular and coarse script respectively. Secondly, despite partial transformation of each to the equilibrium  $(FeMn)Al_6$  phase the major phases remain present during ingot and sheet processing. The varying sizes of these phases at final gauge are less likely to be a consequence of the as cast particle size but more realistically are due to the plastic deformation behaviour of each intermetallic and its crystallography.

#### Mechanical Property Evaluation.

The intrinsic properties (strength and formability) of the lacquered sheet variants were measured in the laboratory using common techniques to simulate a range of strain paths, including uniaxial tension and balanced biaxial tension. In addition the failure energies of the alloy variants were investigated using the Kahn Tear (Navy Tear) test and the double edge notch tensile (D.E.N.T) test (4). The tensile strength of the endstock was largely unaffected by the change in Si content despite the increasing loss of Mg from solid solution in the form of  $Mg_2Si$  particles. In contrast, the sheet tensile ductility was gradually reduced by increasing Si, see figure 5 which shows the serrated flow during tensile testing of these high Mg alloys meant it was impossible to separate the elongation into uniform and necking strains. Values of ~8% are typical for AA5182 endstock tensile tested in the longitudinal orientation. Other

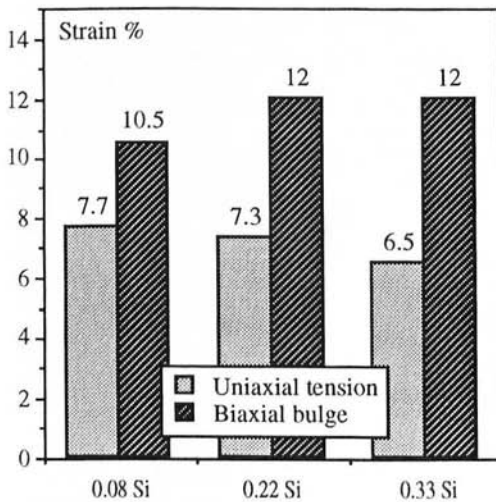


Figure 5: Effect of Si on Strain to Failure.

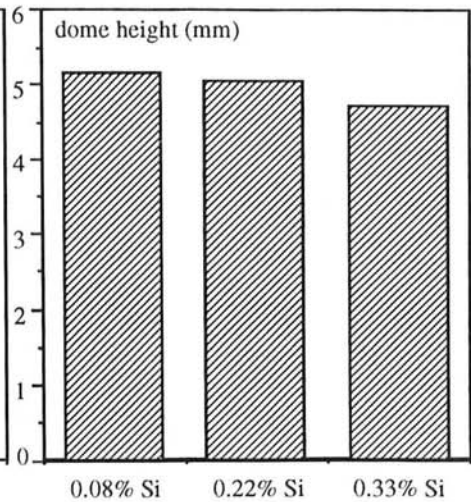


Figure 6: Erichsen Test Performance.

orientations, transverse and diagonal to the rolling direction, give significantly higher values of approximately 12-14%. In the current investigation, the effect of Si is reflected in all orientations. Figure 5 also shows the results from balanced biaxial straining, using a hydraulic bulge tester, and in this instance no consistent influence of composition was determined. This observation is reflected in the performance of the alloys in the standard Erichsen formability test, as shown in Figure 6, which again measures biaxial ductility, and shows only a small effect of Si on sheet performance. These observations are of some interest since the common failure mode of AA5182 endstock is during the formation of the rivet leading to a 'rivet leaker' which is essentially a balance biaxial straining operation. Most commonly, fracture occurs on the dome of the rivet at 90° to the rolling direction during can end manufacture.

The Kahn Tear (or Navy Tear) test uses a single notch specimen strained in a tensile mode such that a tear propagates from the notched side until failure, generating only a small plastic zone ahead of the crack. The load-displacement trace allows the calculation of a propagation energy during failure. Figure 7 shows the unit propagation energy (UPE) for the 3 trial alloys with increasing Si contents. A small degradation in performance was noted when the Si level doubled from 0.1 to 0.2wt% but a more significant drop occurred in sheet with the highest Si addition.

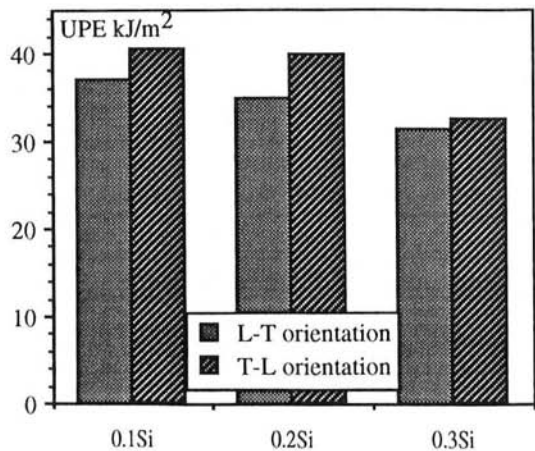


Figure 7: Effect of Si Content on Kahn Tear Energy.

The D.E.N.T. test also measures the energy associated with failure but uses symmetrical, double notched tensile

specimens and the test thus proceeds by the initial formation of a plastically deformed region between the notches (assuming the intrinsic ductility of the material is sufficient) followed by failure. The depth of the notches is varied and the energy required to cause failure is determined in the same fashion as for the Kahn Tear test discussed previously. Because of this sequence of deformation followed by failure, the data from the test may be analysed to give the energy associated with plastic deformation prior to failure and the energy associated with the failure process itself (see (4)). The data are normally represented graphically by plotting the energy per unit area of the notched part of the specimen as a linear function of ligament length between the notches, and the data for the three alloy variants are shown in figure 8.

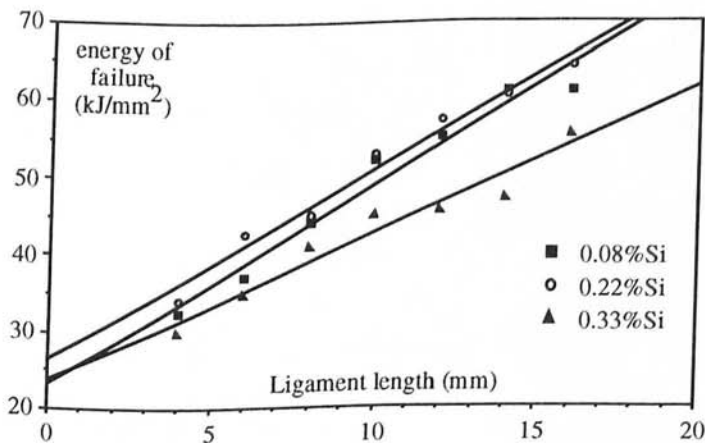


Figure 8: D.E.N.T data for the alloys (for discussion see text).

In such a plot the two key features are the intercept of the line on the ordinate which gives the energy associated with fracture, and the slope of the line drawn through the data, which gives the energy dissipated by plastic deformation prior to failure. The data shown in Figure 8 indicate that the most significant effect of Si occurs at the higher addition of 0.33% and is seen in the reduction in plastic deformation prior to failure, with little significant change in the energy of fracture.

The intrinsic sheet properties have shown that endstock performance gets worse with the addition of Si. Although this is not unexpected from historical data, the magnitude of the effect is somewhat surprising. The major changes in Si in the 3 alloys had been expected to create significant changes in the material properties of the alloys. This perception had come about from the significantly higher volume fraction of coarse magnesium silicide particles predicted and observed in these alloys. The presence of coarse particles is known to influence fracture behaviour and hence tensile properties (2) through the simple concept of void nucleation and growth. This effect is often magnified in hard rolled products because of the particle fracture and voiding that usually occurs during cold rolling (1). Growth of the pre-existing voids is all that then remains for failure to occur and this will be more pronounced in strain paths that encourage strain localisation, ie plane strain. The AA5182 variants studied in this work contained  $Mg_2Si$  volume fractions of approximately 0.2, 0.5 and 1.0%. This phase is also the coarsest at final gauge, with an average size of  $1.4\mu m$ , when compared to the Fe bearing phases. These factors support the above analysis that formability should be extremely poor but this is clearly not the case. A feature of the microstructure that may help explain this observation is the Fe containing particulate. In the previous section, it was shown that the increased Si content effectively reduced the  $N^\circ$  density of coarse particles, greater than the  $0.7\mu m$  limit imposed. The net effect is that the total  $N^\circ$  density of coarse particles,  $Mg_2Si + Fe$ , increases very little from 0.1 to 0.2 wt% Si and by only a small amount increasing to 0.3 wt% Si, despite the direct influence on  $Mg_2Si$ . This implies that the total  $N^\circ$  of coarse particles is the parameter of prime importance and that other features such as average particle size are secondary.

Metallographic sections through tensile strained sheet reveal further evidence of the link between

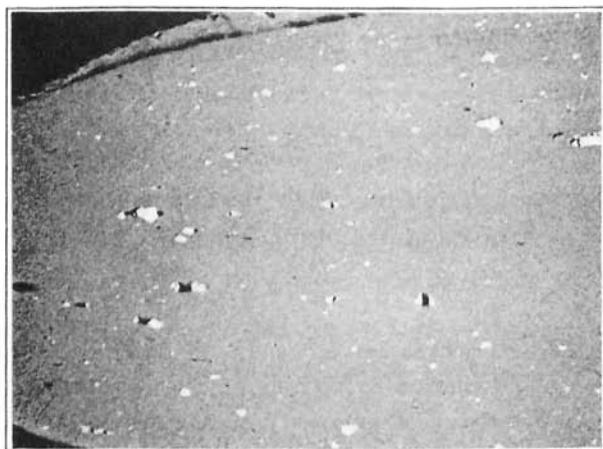


Figure 9: Void formation at Coarse Particles, 25 $\mu$ m

formability and microstructure in AA5182. During straining, voids open up around the hard, second phase particles and eventually coalesce to cause fracture, as shown in Figure 9. Thus the number density of second phase particles will influence significantly the initiation of fracture since this will affect the number, and hence spacing, of the voids. In contrast, the average size of the second phase particles would be expected to influence the onset of fracture only slightly, since this would not significantly change the interparticle spacing. Thus the net effect of increasing Si is seen to affect the onset of fracture by void coalescence in the alloy

containing 0.33 wt%Si where the more significant increase in  $N^{\circ}$  density of particles was observed. This is also seen in the D.E.N.T. data, where only small changes in fracture energy were seen, although a reduction in the plastic work term was observed for the high Si containing alloy. This decrease in the amount of plastic work before fracture could well be manifest as a reduction in formability during can end manufacture.

### Conclusions

- The addition of significant amounts of Si to AA5182 has a profound effect on the coarse particle content of the microstructure. Firstly, the volume fraction of  $Mg_2Si$  dramatically increases and secondly, more surprisingly, the size of Fe containing particles increases with more Si. This latter feature is brought about by the formation of  $\alpha-Al_{15}(FeMn)_3Si_2$  at high Si concentrations.
- The significant change in Si, and thus the microstructure, did not have the expected major influence on sheet formability. The data suggest that it is the total  $N^{\circ}$  density of coarse particles that controls fracture behaviour when strain localisation predominates.
- The drop in formability at high Si levels has been shown to be associated with the change in plastic deformation required before the onset of fracture. This appears to be controlled by the total  $N^{\circ}$  density of hard second phase particles and the presence of voids in strain hardened sheet.

### References

1. R.E. Sanders Jr., D.J. Lege and T.L. Hartman, Aluminium, 65, (1989), 941-947.
2. D.J.Lloyd, Metallurgical Transactions, 11A, (1980), 1287-1294.
3. L.F. Mondolfo, Aluminium Alloys: Structure and Properties, (Butterworths, London 1976), 566-575.
4. H.D. Dudgeon et al, These proceedings.